LAWRENCE
LIVERMORE
NATIONAL
LABORATORY

UCRL-JRNL-202116

Near-infrared Adaptive Optics Imaging of the Satellites and Individual Rings of Uranus from the W.M. Keck Observatory

S. G. Gibbard, I. de Pater#, H. B. Hammel

January 30, 2004

Icarus

Disclaimer

This document was prepared as an account of work sponsored by an agency of the United States Government. Neither the United States Government nor the University of California nor any of their employees, makes any warranty, express or implied, or assumes any legal liability or responsibility for the accuracy, completeness, or usefulness of any information, apparatus, product, or process disclosed, or represents that its use would not infringe privately owned rights. Reference herein to any specific commercial product, process, or service by trade name, trademark, manufacturer, or otherwise, does not necessarily constitute or imply its endorsement, recommendation, or favoring by the United States Government or the University of California. The views and opinions of authors expressed herein do not necessarily state or reflect those of the United States Government or the University of California, and shall not be used for advertising or product endorsement purposes.

Near-infrared Adaptive Optics Imaging of the Satellites and Individual Rings of Uranus from the W.M. Keck Observatory*

S.G. Gibbard[1],I. de Pater[2], H.B. Hammel[3]
[1]Lawrence Livermore National Laboratory
Livermore, CA 94550 USA
sgibbard@igpp.ucllnl.org
[2]Astronomy Department, 601 Campbell Hall
University of California, Berkeley, CA 94720
[3]Space Science Institute
4750 Walnut Street, Suite 205
Boulder, CO 80301

* Data presented herein were obtained at the W.M. Keck Observatory, which is operated as a scientific partnership among the California Institute of Technology, the University of California and the National Aeronautics and Space Administration. The Observatory was made possible by the generous financial support of the W.M. Keck Foundation.

Abstract

We present the first Earth-based images of individual faint rings of Uranus, as observed with the adaptive optics system on the W.M. Keck II Telescope on four consecutive days in October 2003. We derive reflectivities based on multiple measurements of 8 minor moons of Uranus as well as Ariel and Miranda in filters centered at wavelengths of 1.25(J), 1.63(H), and 2.1(Kp) μm. These observations have a phase angle of 1.84-1.96°. We find that the small satellites are somewhat less bright than in observations made by the HST at smaller phase angles, confirming an opposition surge effect. A decrease in flux at Kp band vs. J and H is detected for both the large satellites and several smaller ones (Puck, Portia, Juliet, Cressida, Bianca, and Rosalind), suggestive of the presence of water ice on the surface of these bodies. We calculate albedoes for the ring groups and for each ring separately. We find that the ϵ ring particles, as well as the particles in the 3 other ring groups, have albedoes near 0.043 at these phase angles. The equivalent depths of the individual rings are different than predicted based upon ring widths from occultation measurements (assuming a constant particle ring brightness); in particular the γ ring is fainter and the η ring brighter than expected. Our results indicate that q, the ratio of ϵ ring intensity at apoapse vs. periapse, is close to 3.2$\pm$0.16. This agrees well with a model that has a filling factor for the ϵ ring of 0.06 (Karkoschka 2001, *Icarus* **151**, 78-83). We also determine values of the north to south brightness ratio for the individual rings and find that in most cases they are close to unity.

1. Introduction

Observations of the Uranian system, both from the Earth and from the Voyager 2 spacecraft in 1986 (Smith *et al.* 1986, Stone and Miner 1986), have revealed a number of satellites as well as an extensive ring system. The Uranus ring system consists of groups of narrow annuli in the planet's equatorial plane, interior to $\sim 2R_U$. The outermost ϵ ring ranges in width from 20 km at periapse to 96 km at apoapse. There are three other ring groups interior to the ϵ ring, consisting of narrow rings with widths between 2 and 12 km. The shepherding moons Cordelia and Ophelia confine the ϵ ring (Porco and Goldreich 1987), and other undetected shepherd moons may confine the other rings. Voyager observations, in combination with stellar occultation data, indicate that the rings consist of primarily >cm size particles (French *et al.* 1991). Their spectra are flat at visible and near-infrared wavelengths, and their albedoes are quite low.

The small angular separation between Uranus and its rings (42000 km, <4"), as well as between the rings themselves ($\leq$2700 km or 0.2" between groups, $\leq$1000 km or 0.08" between individual rings) makes it difficult to discern details of the ring structure from ground-based telescopes. Uranus' faint rings and close moons are difficult to detect at visible wavelengths due to scattered light from the planet, but can be more easily observed at wavelengths near 2 μm, where the planet appears dark due to strong methane absorption. Baines *et al.* (1998) and Sromovsky *et al.* (2000) published ground-based images of Uranus and its rings in which the ϵ ring with its asymmetric brightness distribution was easily observed, but due to the relatively low spatial resolution (typically $\sim$ 0.5" from the ground) none of the other rings could be seen. Karkoschka (2001a) published photometry of the Uranian moons and ring system from Hubble Space Telescope images, including the ϵ ring and the three inner ring groups at visible to near-infrared wavelengths.

De Pater *et al.* (2002) presented Keck adaptive optics (AO) observations of the Uranian system, which were taken soon after the AO system became a facility instrument. Since their

field of view was 4.5", they mosaicked Uranus to form a complete picture of the planet and its rings. Their images clearly revealed the ϵ ring and the three inner ring groups. During their observations, the observers noted that extended objects can introduce artifacts in an AO system with a quad-cell Shack-Hartmann sensor, as described in detail in their paper. In response to this, the Keck AO team implemented a procedure which optimizes the AO system for extended objects (van Dam *et al.* 2003,2004).

We report here on observations of Uranus from Keck in October 2003, which show that use of the newly-optimized AO system led to greatly improved Strehl ratios, and hence better image quality. During these observations we achieved a Strehl ratio of 0.5 and a spatial resolution of ≤ 0.05". This is sufficient to resolve (for the first time from an Earth-based image) individual annuli including the α, β, γ, η, and δ rings. We present photometry of the individual Uranian rings, as well as the satellites Miranda, Ariel, and eight smaller moons, and compare our findings to the results of Karkoschka (2001a) and de Pater *et al.* (2002).

2. Observations

We observed Uranus with the 10-m W. M. Keck II telescope[1]on Mauna Kea, Hawaii, on October 3-6 2003 (UT). Images were obtained using the NIRC2 camera, a 1024x1024 Aladdin-3 InSb array[2] . We obtained a typical spatial resolution of 0.043-0.051 arcseconds on nearby stars (which corresponds to about 700 km at Uranus) at all wavelengths observed. Our ring observations are summarized in Table 1; characteristics of the filters are shown in Table 2.

The images were reduced using standard infrared techniques: they were flatfielded using twilight and dome flats, bad pixels were removed (replaced with the median of neighboring

[1] The Keck telescope is jointly owned and operated by the University of California and the California Institute of Technology.

[2] Designed by Keith Matthews and Tom Soifer, both of Caltech. The instrument was built by Keith Matthews and engineer Sean Lin of Caltech, with help from James Larkin, Ian McLean, and others at UCLA (detector electronics and related software), and Al Conrad, Bob Goodrich, and Allan Honey at Keck Observatory (software). Support in Waimea was provided by Jim Bell, Randy Campbell, and Drew Medeiros.

pixels), and the sky was subtracted using a separate image of the sky taken just prior or after the Uranus exposure itself. Figure 1 shows images of the Uranus system for October 5 and 6 2003. On these dates we took single long exposures (600 seconds) of the Uranian ring system, which produced the clearest ring separation of any of our images. These were the images used for the modeling of the ring system (discussed below). Since the disk of Uranus decreases in brightness from J to Kp due to strong methane absorption at Kp, and the ring reflectivities do not vary much with wavelength, the rings are more easily seen at Kp band. Several of the Uranian moons are also visible, particularly at Kp band (labeled in fig. 1). The ϵ ring is easily separated from the other rings within our resolution; the three rings groups are also clearly resolved. The α and β rings are just resolved at a separation of 0.07", and the δ, η, and γ rings are also resolved at separations of 0.06 and 0.10". The 456 rings, although clearly extended, are unresolved. Numerous bright features are visible on the disk of Uranus near the South Polar bright band and at high northern latitudes, as previously reported by Karkoschka (1998) and Hammel *et al.* (2001). There are also features near the equator, at latitudes where such activity has never been detected before. The dynamics and wind velocity profiles of these features will be the subject of a future paper.

3. Satellite Photometry

Photometry of adaptive optics images requires an assessment of the amount of light from the observed object that is concentrated in the centermost 0.3" (the approximate radius of control for the Keck adaptive optics system) and the residual light that is spread into a 'halo' that extends out to an arcsecond or more. In a crowded field with considerable scattered light from Uranus, it is important to use a small photometric aperture, while at the same time accounting for the missing flux from the object. In order to do this, we used a 'bootstrap' procedure as follows: a photometric standard star was observed in "open loop" (non-AO) mode (this star was too bright to be observed in AO mode) and the total counts for the star were calculated. This was used for the conversion of data counts to actual flux. We also observed a point spread

function (PSF) star in AO mode. Using apertures of 1.5" (which contains essentially all the flux from the PSF) and 0.5" we calculated the ratio of the total flux from the PSF to the ratio contained within 0.5" (for our data this ratio was 1.2). For photometry of the large satellites of Uranus (Ariel and Miranda), we determined the number of counts within an aperture of 0.5", then multiplied this by the factor 1.2 to get the total counts. We then used variable apertures on Ariel and Miranda ranging from 0.15 to 0.5", and calculated the ratio of the fraction of light within the smaller apertures to the ratio at 0.5". This provided us the conversion factor for counts on the smaller moons at the decreased aperture size. This ratio was found to be fairly consistent from image to image for a small aperture size of 0.20 arcseconds (ratio of 1.5 for an aperture of 0.5" vs. 0.2"). We therefore used this aperture size and ratio for the other satellites of Uranus. In cases where the brighter satellites Puck and Portia were located close to the planet and there was considerable scattered light, we estimated the contribution of the scattered light using an aperture of the same size in an area that had a similar background flux (this was necessary for some satellites at H and J band, but not at Kp where scattered light from the planet is minimal). For the fainter satellites we did not attempt to calculate a brightness for satellites close to the planet.

Table 3 shows reflectivities for each observed moon on all four nights of observation. Table 4 gives averages and error estimates for the reflectivities of the satellites. In cases where satellites were observed at least three times at a given wavelength, the errors bars were constructed from the standard deviation of the measurements, added in quadrature to the estimated photometric error (5%). For satellites with only one or two observations at a given wavelength, errors were estimated as the sum in quadrature of the photometric error and the estimated noise. Noise was estimated for each image as the average of the noise in apertures at intervals of 20° at a distance of 1" from the planet. Separate estimates were made using apertures of size 0.2" and 0.5". The noise estimate for the larger aperture was used for Ariel and Miranda, while the estimate for the smaller aperture was used for the other satellites.

Since our observations were made at a phase angle of 1.84-1.96°, they are complementary to the low phase angle measurements ($< .1°$) made at these wavelengths by Karkoschka (2001a). Karkoschka found the brightness of the satellites to be higher at phase angles near 0°, which indicates an "opposition surge." We find that the reflectivities of all the Uranian satellites we observed (with the exception of Bianca and Desdemona, for which we have incomplete data), are not constant across wavelength, but instead are considerably brighter at H band than at J or Kp (fig. 2). The decreased flux of the larger Uranian satellites at Kp has previously been attributed to water ice (Brown and Cruikshank 1983), and this is likely to be the case for the other satellites as well. A marginal detection of water ice on Puck was made by Karkoschka (2001a), based on a dip in its spectrum at 2.03 μm. Our observations confirm this detection for Puck, and, based on our measurements, we report evidence for the presence of water ice on the satellites Portia, Juliet, Cressida, Belinda, and Rosalind as well. In contrast to the strong color variation in the Uranian satellites, the rings show very little if any measurable color variation across this wavelength range (see §4 below), indicating an absence of exposed water ice on the surface of the ring particles. The reflectivity of the planet itself (fig. 2, first panel) is a strongly decreasing function of wavelength. Our values for the disk reflectivity (0.016 at J, 0.0095 at H, and 0.00016 at Kp) agree very well with those found by de Pater *et al.* (2002) (0.015 at J, 0.0090 at H, and 0.00016 at Kp).

4. Rings

4.1 Ring Particle Reflectivities

Determining the amount of light that comes from each of the rings is complicated by the effects of the non-symmetric and time-varying PSF and the light scattered from the planet and the bright ϵ ring. In order to account for these effects we constructed a model of the planet

and ring system. This consisted of a (spherical) planet with constant brightness[1](equal to the average I/F of Uranus), and the nine rings: ϵ, δ, γ, η, β, α, 4, 5 and 6. Each ring was represented as a single-pixel-wide ellipse at its appropriate distance from Uranus. Since most pixels have only a fraction of the ellipse passing through them, we assigned to each pixel a value equal to the fraction of the ellipse that occupies it. Each ring was then assigned a brightness that could be varied to get the best fit to the data. Another free parameter was the azimuthal gradient in brightness in the ϵ ring. The other rings were assumed to be azimuthally invariant; this assumption was tested as described below in §4.2. The ring + planet model (the planet is important here as a source of scattered light) was then convolved with the PSF of a reference star at the appropriate wavelength.

The best fit parameter we chose to compare our model to was an average 'slice' of the data constructed by deprojecting the data on a latitude-longitude grid and averaging across the ring system. The actual comparison was made to the difference between the data and a 30-pixel smoothed image, which helps to remove the effects of scattered light. The same procedure was applied to the ring model. Since the effects of scattered light from the ϵ ring are minimized at periapse, the slice was constructed using an average projection of $\pm 5^\circ$ from the northern ansa of the rings (which is close to the periapse of the ϵ ring; see fig. 4 below). This model slice was compared to the data slice and the values of all ten model parameters were varied (using the IDL amoeba routine) until a best fit was reached. The procedure was similar to that used in de Pater *et al.* (2002). Comparisons of the data and model slices are shown in fig. 3 (a-d).

In order to convert the ring brightness parameters in our model into actual ring particle brightnesses, we considered the visible area of the rings. The area of the rings that is visible at a given time is a function of the subsolar latitude and the phase angle of observation. Karkoschka (2001b, fig. 6) gives fractional visible areas for the rings of Uranus. For our observations at a

[1] Due to the smoothing and subtracting procedure discussed below, the results are quite insensitive to the shape of the planet or the value of the planet's reflectivity; for example, a change in the planet's I/F of 100% produces a $< 1\%$ change in the ring brightness, small compared to the error in the observations.

sub-Earth latitude of 18.8-19.6°, the visible fractions are approximately: 0.3 for the ϵ ring; 0.55 for $\alpha\beta$; 0.5 for $\eta\gamma\delta$; and 0.65 for 456. Multiplying these factors by the areas given in Table 1 of Karkoschka (2001b), which are based on equivalent depths from French *et al.* (1986), gives the visible ring areas. We then construct a particle reflectivity by multiplying the modeled ring I/F by the ratio of the actual visible area to the modeled ring area.

Table 5 gives ring particle reflectivities derived from the procedure above for observations on October 5 and 6 at J, H, and Kp bands. Table 6 shows the averages of these six observations. Our nominal model is for the northern ring ansa (to minimize the influence of the scattered light from the ϵ ring), but we also constructed models for the southern ansa, near the ϵ apoapse. The ratio of the brightness of the rings at the southern vs. the northern ansa is shown in Table 5.

Our reflectivities for the ϵ ring particles and for the particles of the three ring groups (ϵ ring=0.043, $\eta\gamma\delta$=0.041, $\alpha\beta$=0.044, 456=0.039) can be compared to values reported by previous observers. Since the rings appear to be grey (this paper, fig. 2, Karkoschka 2001a, de Pater *et al.* 2002), we will compare values without reference to specific wavelengths, considering only the effects of different phase angles. Karkoschka (2001a) found reflectivities of between 0.04 and 0.05 at phase angles of 0.03 to 3°, while Voyager data at larger phase angles indicated a much lower reflectivity of 0.02. Figure 6 from Karkoschka 2001a indicates that, according to his model of the variation of the ring brightness with phase angle, at a phase angle of 2° the ring particle reflectivity should be 0.044. The values we find for the ϵ ring and the three ring groups are in good agreement with this. De Pater *et al.* (2002) reported the following H-band reflectivities at a phase angle of 2.82°: ϵ ring=0.042, $\eta\gamma\delta$=0.042, $\alpha\beta$=0.041, 456=0.033. These values are in excellent agreement with our observations. Both our observations and those of de Pater *et al.* suggest that the 456 ring group may have a somewhat lower particle reflectivity than the others, although this finding does not reach the level of statistical significance.

We have also determined the particle brightness of the individual rings (Table 5). Using the equivalent depth values given by French *et al.* (1986), the results that we find for the individual

rings are quite variable (although by averaging over ring groups we find values that are quite close to the value for the ϵ ring). These variations in brightness between the individual rings include a lowered value of the γ ring and an increase in the η ring. A smaller discrepancy is also found for α and β rings, the β ring being brighter than expected and α somewhat fainter. The 5 ring also has a greatly decreased brightness compared to the 4 and 6 rings, but these three rings are not resolved and the error bars are larger.

If we make the assumption that all the ring particles have the same albedo as the ϵ ring, then some of the ring equivalent depths are considerably different than those given by French *et al.* (1986). Table 6 gives values for the equivalent depths of the rings based on the assumption that all rings have the ϵ reflectivity of 0.043. We again assume the fractional visible areas given by Karkoschka (2001b).

4.2 Ring Brightness as a Function of Orbital Phase

The ϵ ring exhibits a large variation in width, ranging from 96 km at apoapse to only 20 km at periapse. Because the optical depth of the ring is greater than 1 at periapse and less than 1 at apoapse, the ratio of the brightness at apoapse to the brightness at periapse, q, is not merely the ratio of the ring widths. The value of q is important as a diagnostic of the "filling factor" D, the fractional volume of the ring occupied by ring particles. Determining the value of D from the observed q requires a model of the ring particles; the model used by many observers is that of Hapke (1981). However, Karkoschka (2001b) used a model by Irvine (1966) that better accounts for the observed increase in brightness caused by reduced ring particle shadowing at opposition. Using this model he predicts that the ratio q will increase from 2 to 5 as Uranus approaches ring plane crossing in 2007.

Svitek and Danielson (1987) found values of q near 2.4 for observations made by the HST. Karkoschka (2001b) gives values of $q \simeq 2.5$ for HST measurements at phase angles between 0.03 and 3. Combining these data with a Voyager measurement at a phase angle of 20° (at larger phase angles q is highly diagnostic of the filling factor D) Karkoschka concludes that a value

of D=0.06 is the best fit to all the data. If we use Karkoschka's result with D=0.06, we would expect q=3.2 for our data at a sub-Earth latitude of -18.9° (Karkoschka 2001b, figure 5). In an analysis of six ring images (Table 5), two each at J, H, and Kp, we find the average value of the south to north ratio to be 3.2±.16, in excellent agreement with Karkoschka's prediction. We note that the north/south ratio is not exactly the same as q, since the periapsis of the ϵ ring was not located exactly at the northernmost edge of the rings (fig. 4); therefore the actual value of q may be somewhat larger than this.

The brightness ratios of the other rings may also vary as a function of ring width, which for some of the rings may be a simple function of longitude. For example, the ϵ, α, β, and δ rings show a simple correlation between the width and orbital phase, with a maximum width occurring near apoapsis (French *et al.* 1991). The gamma ring also shows width variations, but there is no obvious relation to the orbital phase. In our model we varied the brightness of the ϵ ring with orbital phase, but considered the other rings to be of equal brightness at all phases. To test the validity of this assumption we also modeled the data at the southern ansa. As fig. 4 shows, at the time of our observations the periapses of the ϵ, β, 4 and 6 rings were in the northern ansa, while the α ring's periapsis was in the south.

The results indicate (Table 6) that the rings (with the exception of the ϵ ring) do not show any significant variation in brightness from north to south except for a possible increase in brightness of the η ring (which is not known to have a simple orbital phase variation in brightness). This indicates, first, that our modeling is not compromised by the assumption of a constant ring brightness; and second, that variations in the widths of the α and β rings (assuming that these widths are the same as those measured by Voyager in 1986) do not lead to variations in ring brightness. This would be the case if, for example, the rings had a low filling factor such that an increase in ring width would not bring into view a large amount of material that had been hidden in the shadow of other ring particles. Another possibility is that there has been a change in ring width since the occultation measurements were made. Further observations are obviously needed to clarify this point.

5. Conclusions

Our observations of the Uranian satellite and ring system at near-infrared wavelengths have produced the first resolved images of individual faint rings of Uranus, and the first detection of a decrease in reflectivity at 2 microns suggestive of water ice on the Portia group of satellites. We have presented values for the albedo of Uranian satellites in broadband J, H, and Kp filters which are in good agreement with previous values, and confirm the opposition surge found by Karkoschka (2001a).

Our values for the ring group reflectivities are in excellent agreement with previous measurements (de Pater *et al.* 2002, Karkoschka 2001a). We find the ring albedo to be quite flat in the range from 1.17 to 2.3 microns. However, the equivalent depths for individual rings are found to be different from previous values (French *et al.* 1986), if we assume that all the ring particles in the Uranian system have the same brightness.

We find a value of 3.2 for the north/south brightness ratio of the ϵ ring (which is close to the apoapse/periapse ratio q), in good agreement with the Karkoschka (2001b) model with a filling factor of 0.06. For the α and β rings q is close to 1.0, which indicates no significant brightness difference despite an orbital phase variation in ring width. This suggests either that there is relatively little shadowing occurring in these rings, or perhaps that the peripase/apoapse width variation has changed in time. Further observations, especially as Uranus approaches ring plane crossing in 2007 with an expected large increase in q, will help clarify this issue.

Acknowledgements

This work has been supported in part by the National Science Foundation Science and Technology Center for Adaptive Optics, managed by the University of California at Santa Cruz under cooperative agreement No. AST 9876783.

This work was performed under the auspices of the U.S. Department of Energy, National Nuclear Security Administration, by the University of California, Lawrence Livermore National Laboratory under contract No. W-7405-Eng-48.

HBH acknowledges support from NASA grants NAG5-10451 and NAG5-11961.

Data presented herein were obtained at the W.M. Keck Observatory, which is operated as a scientific partnership among the California Institute of Technology, the University of California and the National Aeronautics and Space Administration. The Observatory was made possible by the generous financial support of the W.M. Keck Foundation.

The authors extend special thanks of those of Hawaii ancestry on whose sacred mountain we are priviledged to be guests. Without their generous hospitality, none of the observations presented would have been possible.

Figure Captions

Figure 1: Images of Uranus taken on 5 and 6 October 2003 (UT) in three near-infrared broadband filters. The Kp (2.1 micron) images are shown unaltered; in the J (1.25) and H (1.63) band images the planet's intensity (out to its physical radius) has been reduced by a factor of 30 so that the rings and details of the planet's disk can be shown in the same image. Scattered light from the planet is important at J and H band, but at Kp band methane absorption sharply reduces the light from the planet so that details of the ring structure and the satellites (labeled in the images) can be seen.

Figure 2: Reflectivity vs. wavelength for the disk of Uranus (averaged over 5 and 6 October), ring particles, and several Uranian satellites. Near-infrared values are from this work; the horizontal bars represent the wavelength range of the broadband filters. Values at 0.55 μm are extrapolated from Karkoschka (2001a, fig. 6) to values expected for a phase angle of 1.9°. The ring particles show a very flat spectrum, in contrast to the satellites which all exhibit a decrease in intensity from H to Kp band.

Figure 3: Comparison of averaged ring brightness (averaged over 5° at the northern and southern ansae) to model brightness. Details of the averaging and modeling procedure are discussed in the text. 2a) Data from 5 October, northern ansa. 2b) 6 October, northern ansa. 2c) 5 October, southern ansa. 2d) 6 October, southern ansa.

Figure 4: Appearance of Uranus on 5 October, 9:00 UT. The ring periapses (ϵ, β, 4 and 6 in the north, α in the south) are marked with black dots. Periapses not shown are located behind the disk of the planet. Diagram generated by the Uranus Viewer Tool, PDS Rings Node (*ringside.arc.nasa.gov/www/tools/tools.html*).

References

Baines, K.H., P.A. Yanamandra-Fisher, L.A. Lebofsky, T.W. Momary, W. Golish, C. Kaminski, W.J. Wild 1998. Near-infrared absolute photometric imaging of the Uranian system. *Icarus* **132**, 266-284.

Brown, R.H., and D.P. Cruikshank 1983. The uranian satellites: Surface compositions and opposition brightness surges. *Icarus* **55**, 83-92.

de Pater, I., S.G. Gibbard, B.A. Macintosh, H.G. Roe, D.T. Gavel, and C.E. Max 2002. Keck adaptive optics images of Uranus and its rings. *Icarus* **160**, 359-374.

French, R.G., J.L. Elliot, and S.E. Levine 1986. Structure of the Uranian rings. II. Ring orbits and widths. *Icarus* **67**, 134-163.

French, R.G., P.D. Nicholson, C.C. Porco, and E.A. Marouf 1991. Dynamics and structure of the Uranian rings. *Uranus*, Eds. J.T. Bergstrahl, E.D. Miner, M.S. Matthews. Univ. of Arizona Press, Tucson, AZ. pp. 327-409.

Hammel, H.B., K. Rages, G.W. Lockwood, E. Karkoschka, and I. de Pater 2001. New measurements of the winds of Uranus. *Icarus* **153**, 229-235.

Hapke, B. 1981. Bidirectional reflectance spectroscopy, 1. Theory. *J. Geophys. Res.* **86**, 4571-4586.

Irvine, W.M. 1966. The shadowing effect in diffuse reflection. *J. Geophys. Res.* **71**, 2931-2937.

Karkoschka, E. 1998. Clouds of high contrast on Uranus. *Science* **280**, 570-572.

Karkoschka, E. 2001a. Comprehensive photometry of the rings and 16 satellites of Uranus with the Hubble Space Telescope. *Icarus*, **151**, 51-68.

Karkoschka, E. 2001b. Photometric modeling of the epsilon ring of Uranus and its spacing of particles. *Icarus*, **151**, 78-83.

Porco, C.C., and P. Goldreich 1987. Shepherding of the Uranian rings. I. Kinematics. *Astron. J.* **93**, 724-729.

Smith, B.A., *et al.* 1986. Voyager 2 in the Uranian system: Imaging science results, *Science* **233**, 43-64.

Sromovsky, L.A., J.R. Spencer, K.H. Baines, and P.M. Fry 2000. Ground-based observations of cloud features on Uranus. *Icarus* **146**, 307-311.

Stone, E.C., and E.D. Miner 1986. The Voyager 2 encounter with the Uranian system. *Science* **233**, 39-43.

Svitek, T. and G.E. Danielson 1987. Azimuthal brightness variation and albedo measurements of the uranian rings. *J. Geophys. Res.* **92**, 14979-14986.

van Dam, M.A., and B.A. Macintosh 2003. Characterization of adaptive optics at Keck Observatory. *SPIE* **5169**, 1-10.

van Dam, M.A., D. Le Mignant, and B.A. Macintosh 2004. Performance of the Keck Observatory adaptive optics system. Submitted to *Applied Optics*.

Table 1

Uranus Ring Observations

Date (UT)	Time (UT)	Wavelength	Exposure time (sec)	FWHM
5 Oct 2003	9:06	Kp	300	0.051
5 Oct 2003	9:33	J	180	0.045
5 Oct 2003	9:38	H	300	0.043
6 Oct 2003	5:35	J	180	0.049
6 Oct 2003	9:07	Kp	300	0.045
6 Oct 2003	9:33	H	300	0.045

Table 2

Filter Characteristics

Filter Name	Central Wavelength (μm)	Wavelength Range (μm)
J	1.25	1.17-1.33
H	1.63	1.48-1.78
Kp	2.12	1.95-2.30

Filter traces and further information are available at:
http://alamoana.keck.hawaii.edu/inst/nirc2/filters.html

Table 3

Moon reflectivities

Date (UT)	λ	phase	Ariel	Miranda	Puck	Portia	Juliet	Cressida	Belinda	Rosalind	Desdemona	Bianca
Oct. 3 5:44	J	1.84	-	0.222	-	0.060	-	-	0.040	-	-	-
Oct. 3 9:09	J	1.85	-	-	-	-	0.065	-	-	-	-	-
Oct. 4 5:18	J	1.88	-	-	0.070	-	-	-	0.075	-	-	-
Oct. 4 7:20	J	1.88	-	-	-	0.060	-	-	-	-	-	-
Oct. 4 9:55	J	1.89	-	-	0.066	-	0.042	-	0.080	-	-	-
Oct. 5 5:18	J	1.92	-	0.231	0.057	-	-	-	-	-	-	-
Oct. 5 7:20	J	1.92	-	0.246	0.063	0.045	0.065	-	-	-	-	-
Oct. 5 9:33	J	1.92	-	-	-	0.045	0.052	0.043	-	0.061	-	-
Oct. 6 5:35	J	1.95	0.321	-	-	-	-	-	-	-	-	-
Oct. 6 6:56	J	1.96	-	-	-	0.057	0.056	-	0.069	-	-	-
Oct. 3 5:22	H	1.84	-	0.327	-	0.072	-	-	.107	-	-	-
Oct. 3 9:32	H	1.85	-	-	0.077	-	0.11	-	-	0.11	-	-
Oct. 4 5:03	H	1.88	-	-	0.11	-	-	-	0.058	0.085	-	-
Oct. 4 7:03	H	1.88	-	-	0.074	0.071	0.67	-	0.097	-	-	-
Oct. 4 9:39	H	1.89	-	-	-	0.065	0.086	-	0.088	-	-	0.062
Oct. 5 5:02	H	1.92	-	0.341	0.096	-	-	-	-	-	-	-
Oct. 5 7:00	H	1.92	-	0.347	0.087	0.072	-	-	0.079	-	-	0.043
Oct. 5 9:17	H	1.92	-	-	-	0.057	0.076	0.050	-	0.075	-	-
Oct. 6 5:20	H	1.96	0.438	-	-	-	-	-	-	0.10	0.13	-
Oct. 6 7:11	H	1.96	-	-	0.083	-	0.074	0.073	-	-	-	-
Oct. 6 9:47	H	1.96	-	-	-	0.062	0.047	-	0.052	-	-	-
Oct. 3 5:53	Kp	1.84	-	0.159	-	0.053	-	-	0.043	0.047	-	-
Oct. 3 9:40	Kp	1.85	-	-	0.055	-	0.057	-	-	-	-	0.079
Oct. 4 5:24	Kp	1.88	-	-	0.062	0.044	-	0.049	0.044	0.044	0.066	-
Oct. 4 7:28	Kp	1.88	-	-	-	0.058	0.054	0.052	-	0.056	0.048	-
Oct. 4 10:01	Kp	1.89	-	-	0.069	-	0.053	-	0.051	-	-	0.11
Oct. 5 5:22	Kp	1.92	-	0.164	0.063	-	-	-	-	-	-	-
Oct. 5 7:28	Kp	1.92	-	0.166	0.065	0.055	0.068	-	0.033	-	-	-
Oct. 5 9:06	Kp	1.92	-	0.153	0.063	0.052	-	0.026	-	0.076	-	-
Oct. 6 5:40	Kp	1.95	.213	-	-	-	-	-	0.047	0.043	-	-
Oct. 6 7:17	Kp	1.96	-	-	0.070	0.064	0.079	0.058	-	-	-	-
Oct. 6 9:07	Kp	1.96	-	-	0.057	0.047	0.051	0.058	0.036	-	0.024	-

Table 4

Average Uranus moon reflectivities in the near-IR

Wavelength	Ariel	Miranda	Puck	Portia	Juliet	Cressida	Belinda	Rosalind	Desdemona	Bianca
J (1.25μm)	0.321± 0.018*	0.233± 0.017	0.064± 0.0064	0.053± 0.0082	0.056± 0.010	0.043± 0.006*	0.066± 0.018	0.061± 0.008*	-	-
H (1.63 μm)	0.438± 0.023*	0.338± 0.020	0.088± 0.014	0.067± 0.0071	0.077± 0.021	0.061± 0.015*	0.080± 0.020	0.093± 0.017	-	0.053± 0.02*
Kp (2.12μm)	0.213± 0.012*	0.161± 0.010	0.063± 0.0056	0.053± 0.0072	0.060± 0.011	0.049± 0.013	0.042± 0.0070	0.053± 0.014	0.046± 0.021	0.094± 0.02*

* 1-σ error based on estimated noise and photometery error; all others are photometry error plus standard deviation of multiple observations

Table 5
Ring Particle Reflectivities

Date	Wavelength	Ring (group)	Reflectivity	South/North ratio
Oct. 5 2003	J	ϵ	0.042± 0.009	3.13
		δ	0.060±0.009	1.0
		γ	0.018±0.009	1.46
		η	0.087±0.009	1.55
		$\delta\gamma\eta$	0.045±0.009	-
		β	0.057± 0.009	1.0
		α	0.036± 0.009	1.0
		$\alpha\beta$	0.048± 0.009	-
		4	0.070± 0.009	0.65
		5	0.023± 0.009	0.78
		6	0.058± 0.009	1.0
		456	0.046± 0.009	-
Oct. 5 2003	H	ϵ	0.042 ± 0.007	3.14
		δ	0.047± 0.007	1.04
		γ	0.024± 0.007	1.01
		η	0.051± 0.007	1.03
		$\delta\gamma\eta$	0.037± 0.007	-
		β	0.047 ± 0.007	0.96
		α	0.026 ± 0.007	1.09
		$\alpha\beta$	0.039 ± 0.007	-
		4	0.062 ± 0.007	1.0
		5	0.016 ± 0.007	1.0
		6	0.076 ± 0.007	1.02
		456	0.044 ± 0.007	-
Oct. 5 2003	Kp	ϵ	0.042±0.005	3.36
		δ	0.046± 0.005	0.73
		γ	0.013± 0.005	0.97
		η	0.076± 0.005	1.22
		$\delta\gamma\eta$	0.036± 0.005	-
		β	0.045± 0.005	0.94
		α	0.037± 0.005	0.77
		$\alpha\beta$	0.042± 0.005	-
		4	0.057± 0.005	0.70
		5	0.018± 0.005	0.99
		6	0.039± 0.005	0.99
		456	0.036± 0.005	-

Table 5, cont.
Ring Particle Reflectivities

Date	Wavelength	Ring (group)	Reflectivity	South/North ratio
Oct. 6 2003	J	ϵ	0.045 ± 0.009	2.98
		δ	0.055 ± 0.009	1.38
		γ	0.019 ± 0.009	1.33
		η	0.1 ± 0.009	1.16
		$\delta\gamma\eta$	0.046 ± 0.009	-
		β	0.054 ± 0.009	1.04
		α	0.034 ± 0.009	0.96
		$\alpha\beta$	0.046 ± 0.009	-
		4	0.027 ± 0.009	1.0
		5	0.013 ± 0.009	0.90
		6	0.085 ± 0.009	0.80
		456	0.033 ± 0.009	-
Oct. 6 2003	H	ϵ	0.046 ± 0.007	3.12
		δ	0.051 ± 0.007	1.04
		γ	0.022 ± 0.007	0.64
		η	0.084 ± 0.007	1.50
		$\delta\gamma\eta$	0.043 ± 0.007	-
		β	0.052 ± 0.007	1.04
		α	0.029 ± 0.007	1.30
		$\alpha\beta$	0.043 ± 0.007	-
		4	0.050 ± 0.007	0.54
		5	0.013 ± 0.007	1.04
		6	0.053 ± 0.007	1.60
		456	0.034 ± 0.007	
Oct. 6 2003	Kp	ϵ	0.043 ± 0.005	3.40
		δ	0.038 ± 0.005	1.0
		γ	0.016 ± 0.005	1.0
		η	0.086 ± 0.005	1.12
		$\delta\gamma\eta$	0.036 ± 0.005	-
		β	0.050 ± 0.005	1.0
		α	0.035 ± 0.005	0.90
		$\alpha\beta$	0.044 ± 0.005	-
		4	0.052 ± 0.005	0.77
		5	0.019 ± 0.005	0.80
		6	0.077 ± 0.005	0.76
		456	0.042 ± 0.005	-

Table 6

Average Ring Particle Reflectivities

Ring (group)	Reflectivity	A (km)	A' (km)	South/North ratio
ϵ	0.043± 0.002	95.0	95.0	3.2± 0.16
$\delta+\delta_c$	0.050±0.008	4.99	5.69	1.03± 0.21
γ	0.019±0.004	6.57	3.67	1.07± 0.29
$\eta+\eta_c$	0.081±0.016	2.52	3.70	1.26± 0.21
$\delta\gamma\eta$	0.041±0.005	14.08	13.45	-
β	0.051± 0.004	6.68	7.73	1.0± 0.04
α	0.033± 0.004	4.27	3.47	1.0± 0.18
$\alpha\beta$	0.044± 0.003	10.95	11.2	-
4	0.053± 0.014	1.41	1.58	0.78± 0.19
5	0.017± 0.004	1.81	2.44	0.92± 0.11
6	0.065± 0.018	0.82	0.613	1.03± 0.30
456	0.039± 0.006	4.04	3.71	-

Note: A=equivalent depth (from French *et al.* 1986); A'=equivalent depth assuming that all rings have the ϵ ring particle reflectivity

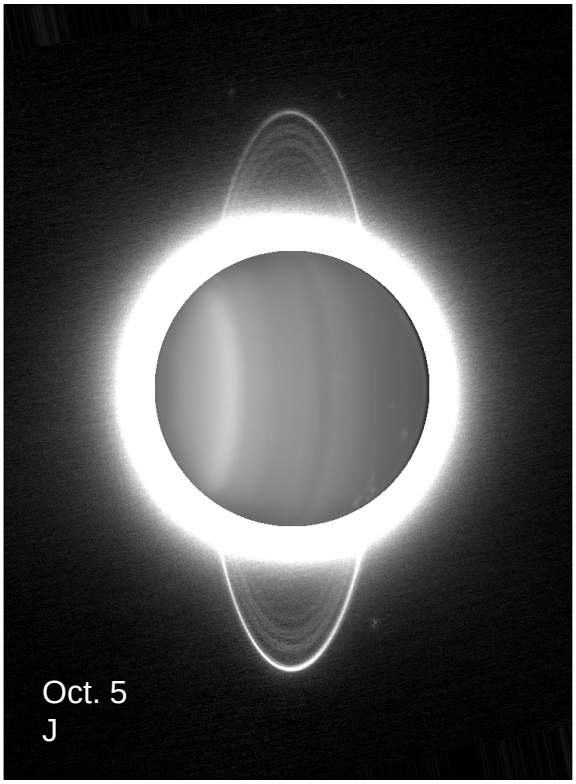
Oct. 5
J

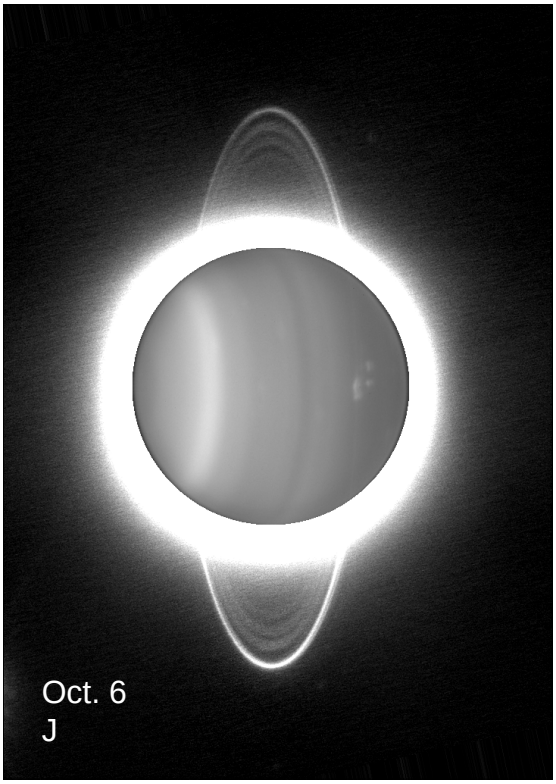
Oct. 6
J

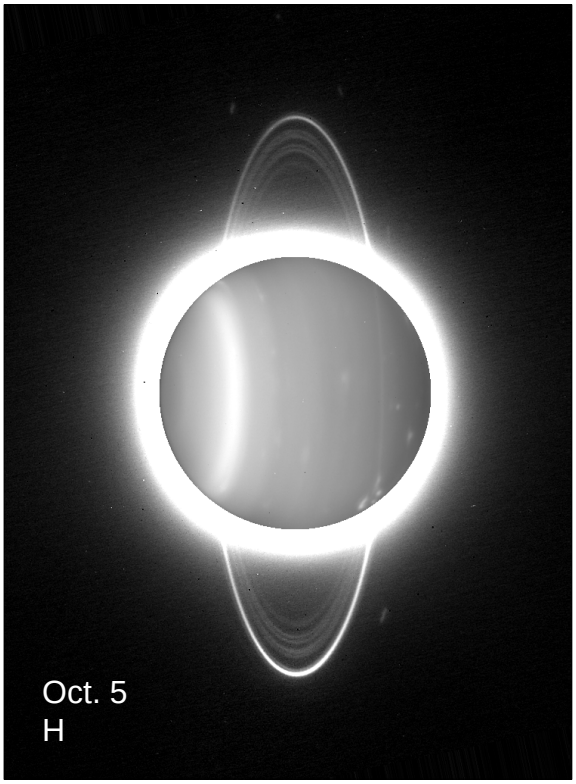
Oct. 5
H

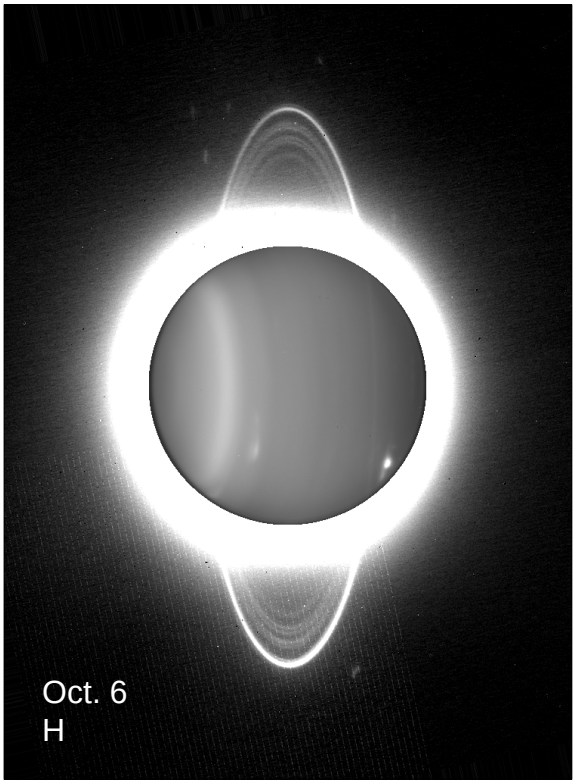
Oct. 6
H

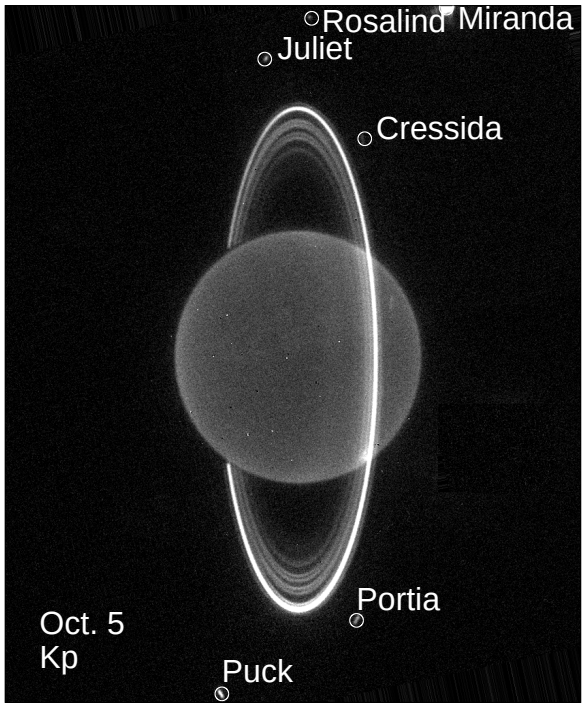
Rosalind
Miranda
Juliet
Cressida
Portia
Oct. 5
Kp
Puck

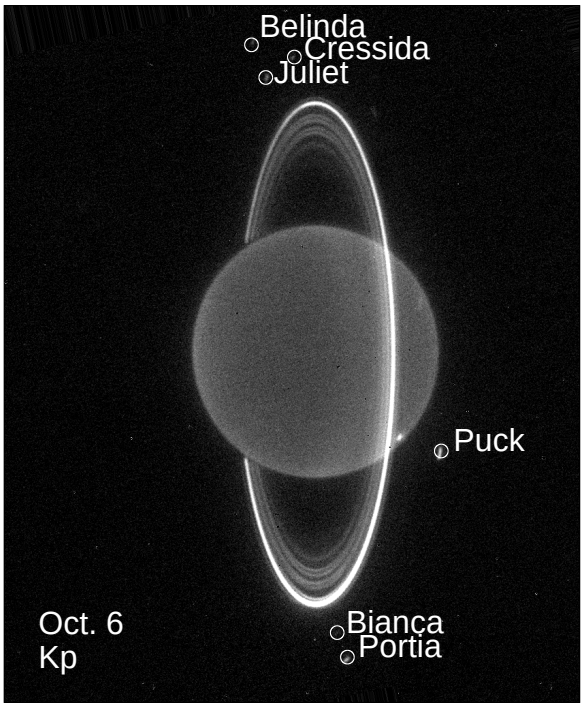
Belinda
Cressida
Juliet
Puck
Oct. 6
Kp
Bianca
Portia

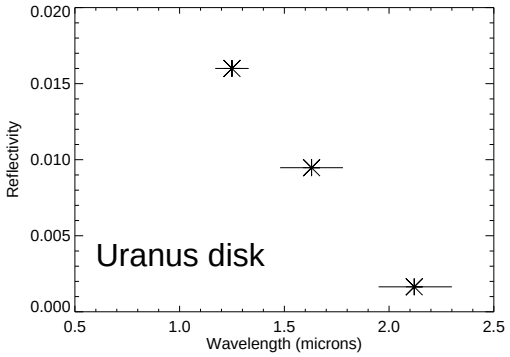
Uranus disk
Reflectivity
Wavelength (microns)
0.020
0.015
0.010
0.005
0.000
0.5
1.0
1.5
2.0
2.5

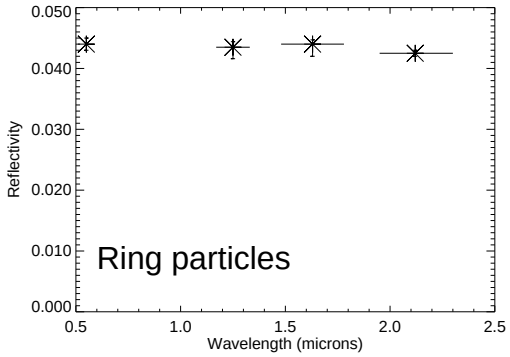
Ring particles
Reflectivity
Wavelength (microns)
0.050
0.040
0.030
0.020
0.010
0.000
0.5
1.0
1.5
2.0
2.5

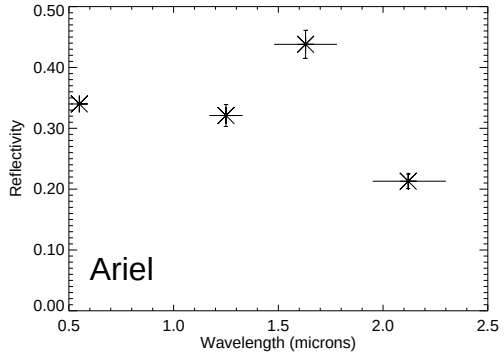
Ariel
Reflectivity
Wavelength (microns)
0.50
0.40
0.30
0.20
0.10
0.00
0.5
1.0
1.5
2.0
2.5

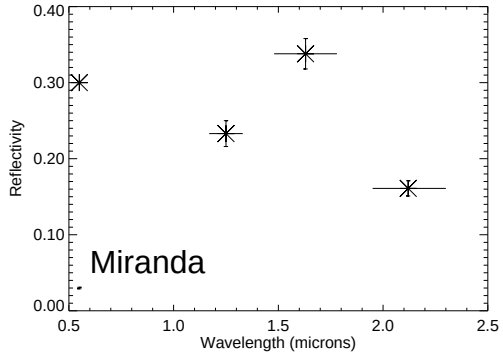
Miranda
Reflectivity
Wavelength (microns)
0.40
0.30
0.20
0.10
0.00
0.5
1.0
1.5
2.0
2.5

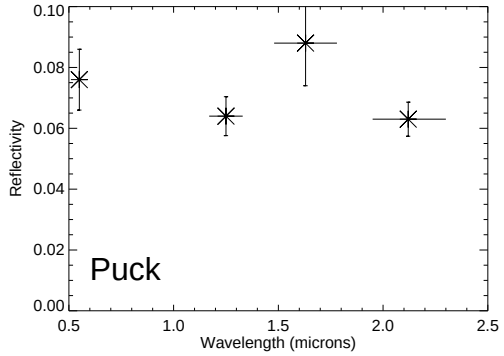
Puck
Reflectivity
Wavelength (microns)
0.10
0.08
0.06
0.04
0.02
0.00
0.5
1.0
1.5
2.0
2.5

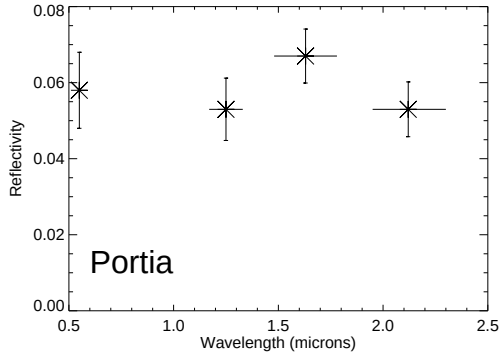
Portia
Reflectivity
Wavelength (microns)
0.08
0.06
0.04
0.02
0.00
0.5
1.0
1.5
2.0
2.5

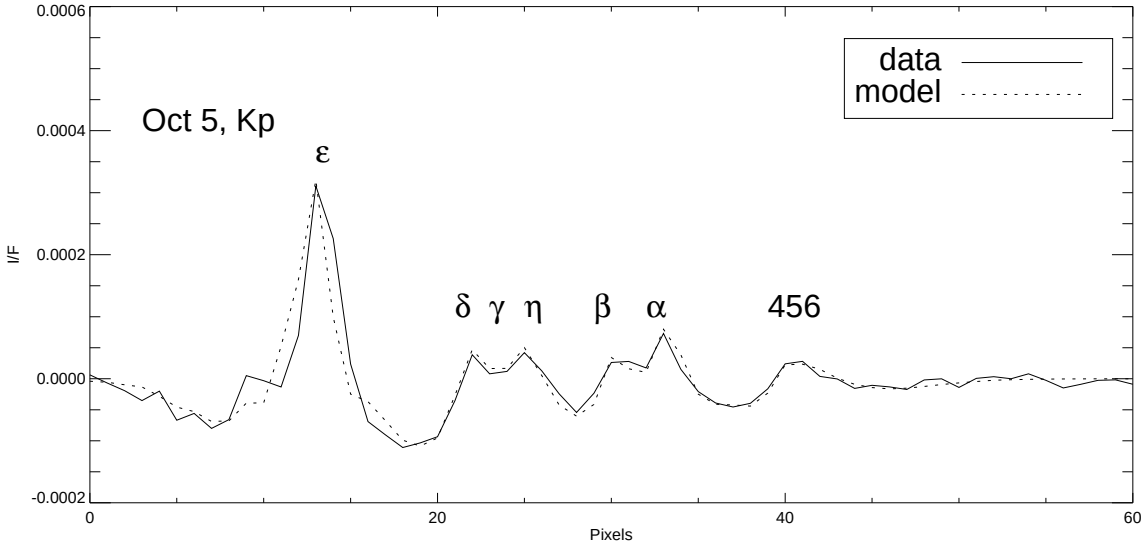
Oct 5, Kp
data
model
ε
δ γ η β α
456
I/F
Pixels
0.0006
0.0004
0.0002
0.0000
-0.0002
0
20
40
60

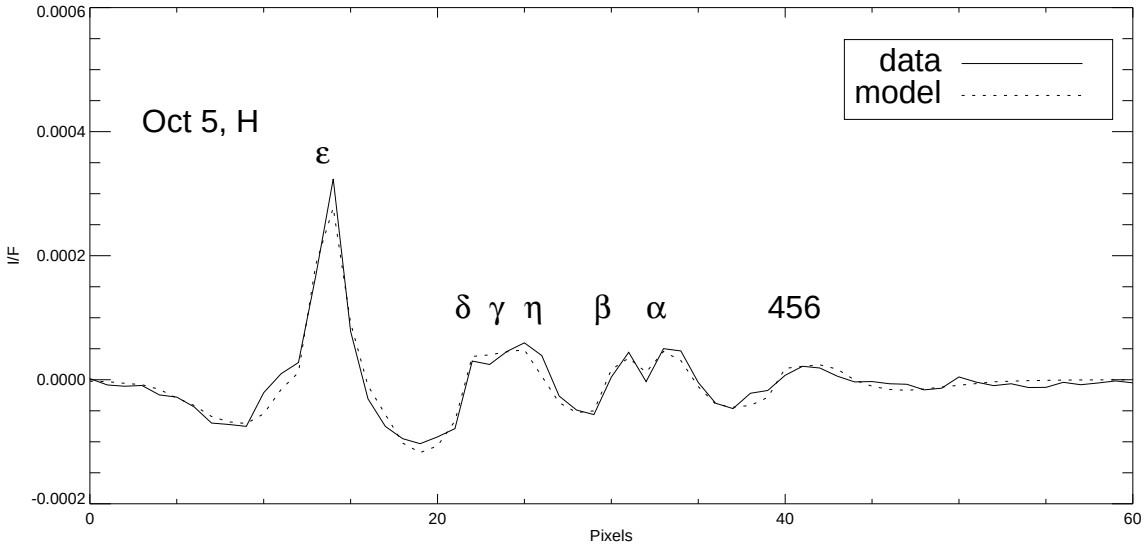
Oct 5, H
data
model
ε
δ γ η β α
456
I/F
Pixels
0.0006
0.0004
0.0002
0.0000
-0.0002
0
20
40
60

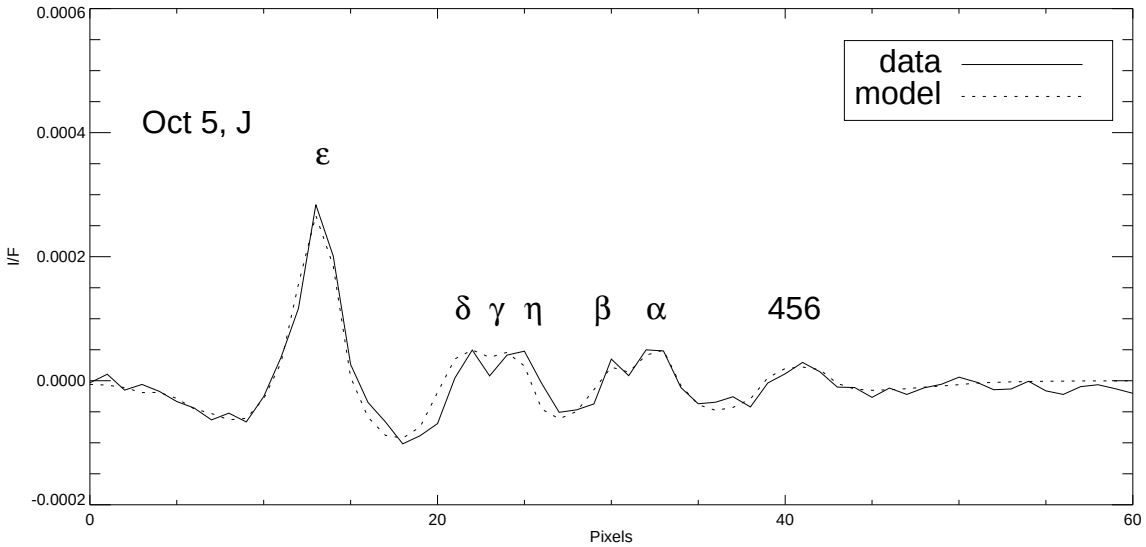
Oct 5, J
data
model
ε
δ γ η β α
456
I/F
Pixels
0.0006
0.0004
0.0002
0.0000
-0.0002
0
20
40
60

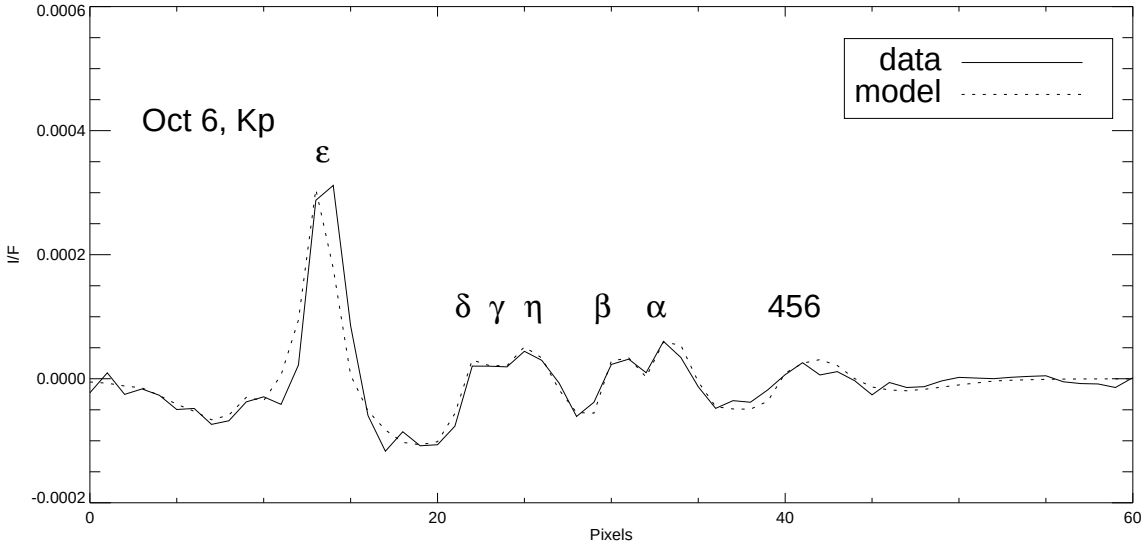
Oct 6, Kp
data
model
ε
δ γ η β α
456
I/F
Pixels
0.0006
0.0004
0.0002
0.0000
-0.0002
0
20
40
60

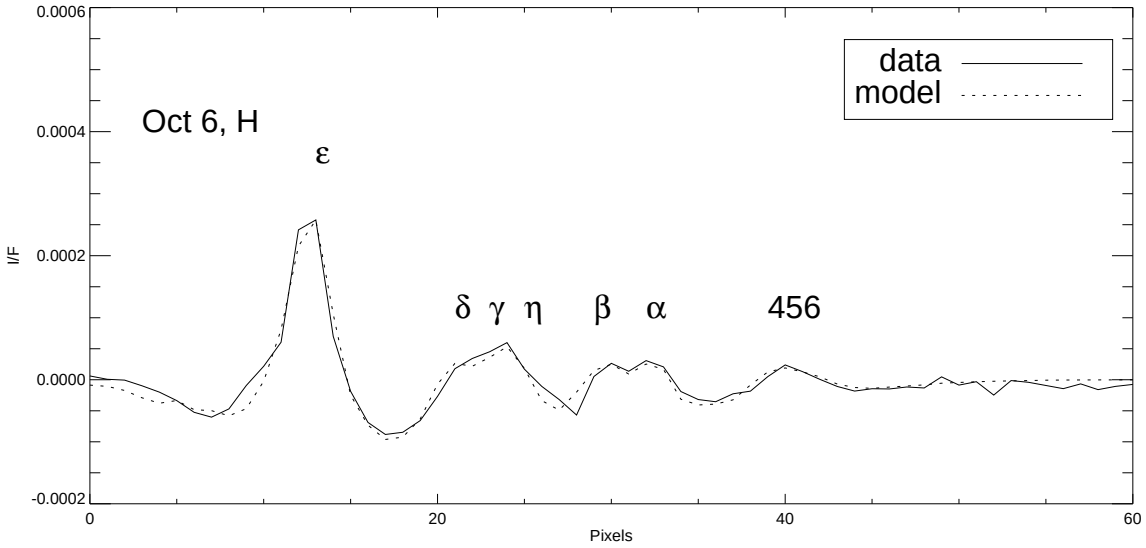
Oct 6, H
data
model
ε
δ γ η β α
456
I/F
Pixels
0.0006
0.0004
0.0002
0.0000
-0.0002
0
20
40
60

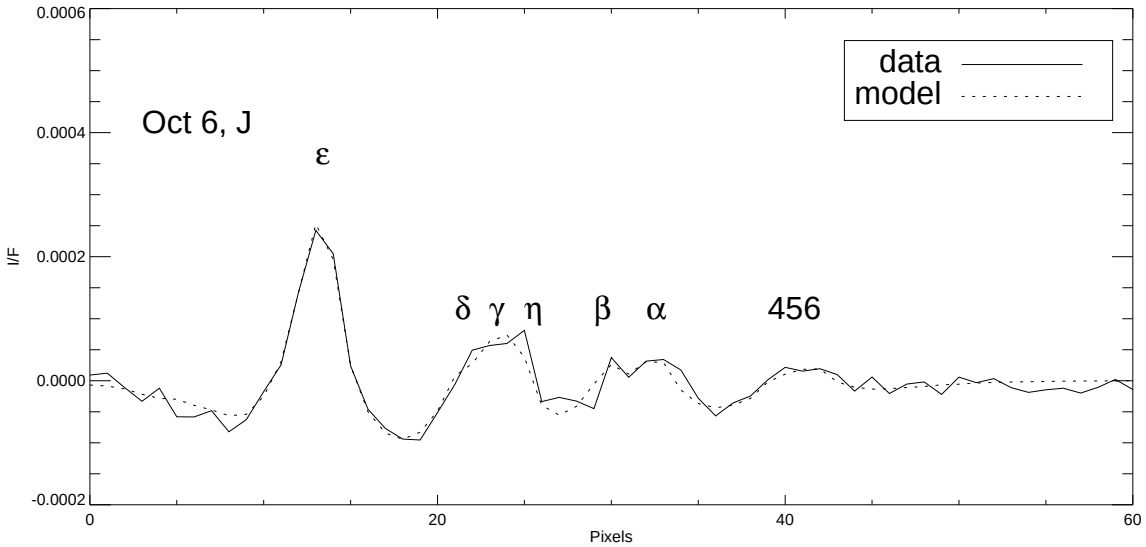
Oct 6, J
data
model
ε
δ γ η β α
456
I/F
Pixels
0.0006
0.0004
0.0002
0.0000
-0.0002
0
20
40
60

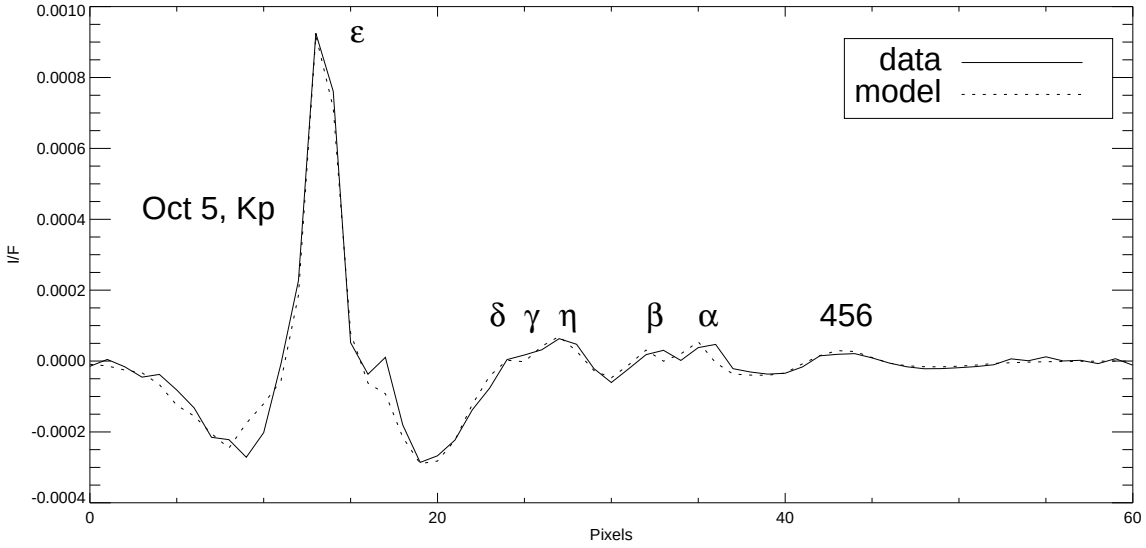
ε
data
model
Oct 5, Kp
δ γ η
β
α
456
I/F
Pixels

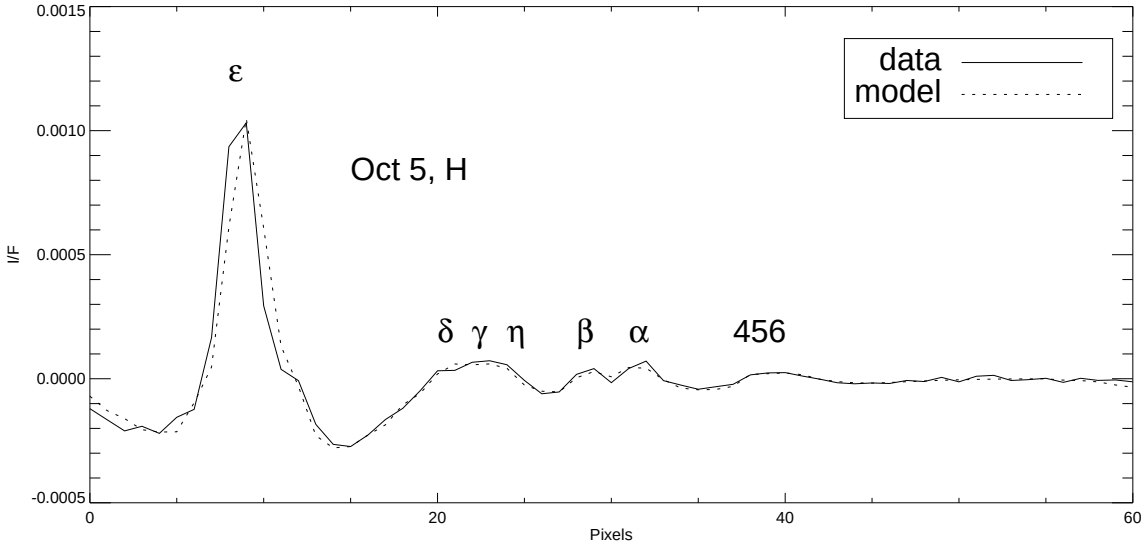
ε
data
model
Oct 5, H
δ γ η
β
α
456
I/F
Pixels

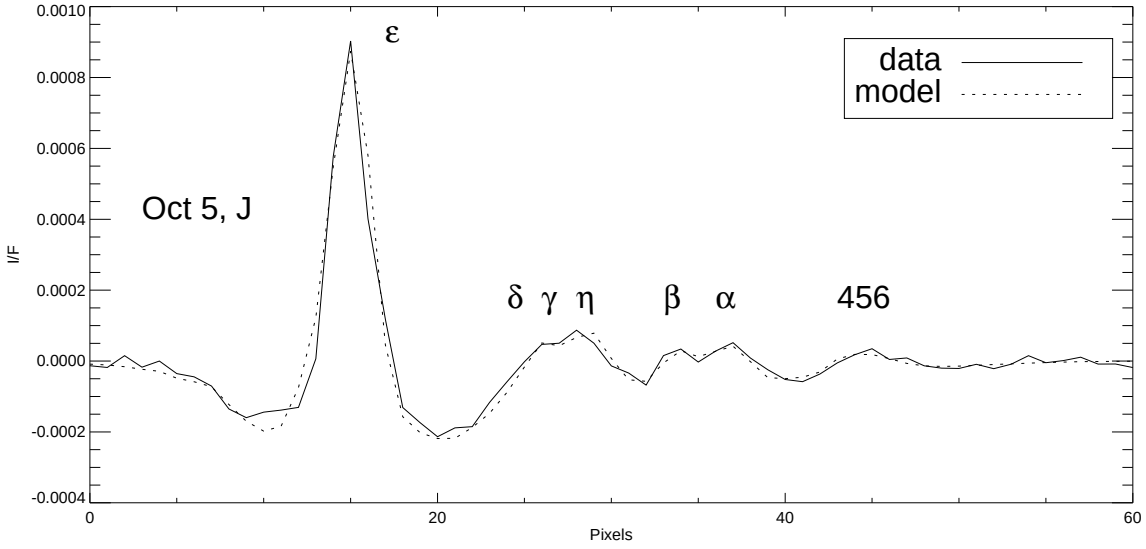
ε
data
model
Oct 5, J
δ γ η
β
α
456
I/F
Pixels

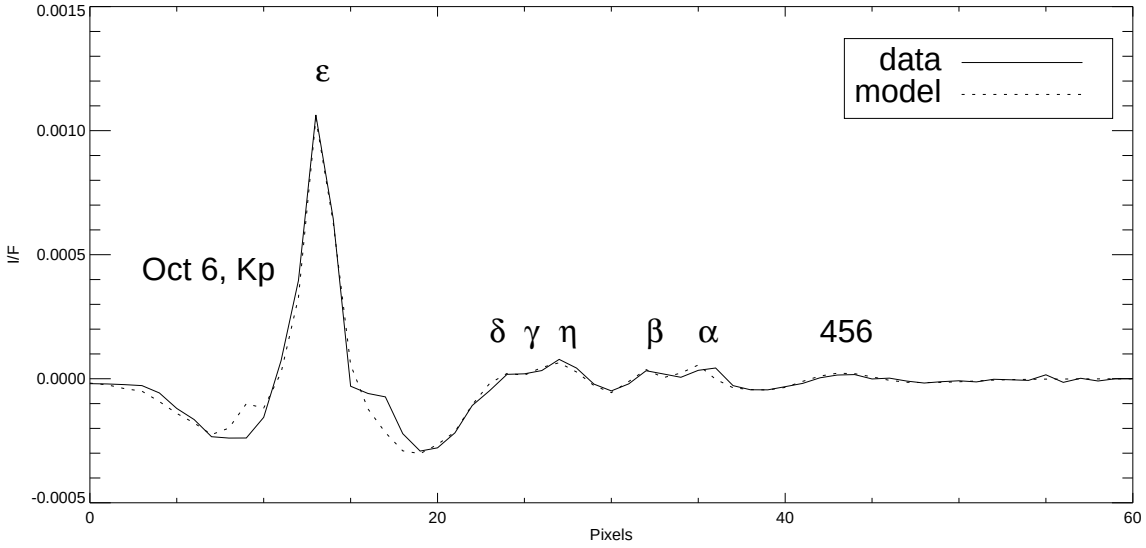
data
model
ε
Oct 6, Kp
δ γ η β α 456
I/F
Pixels
0.0015
0.0010
0.0005
0.0000
-0.0005
0
20
40
60

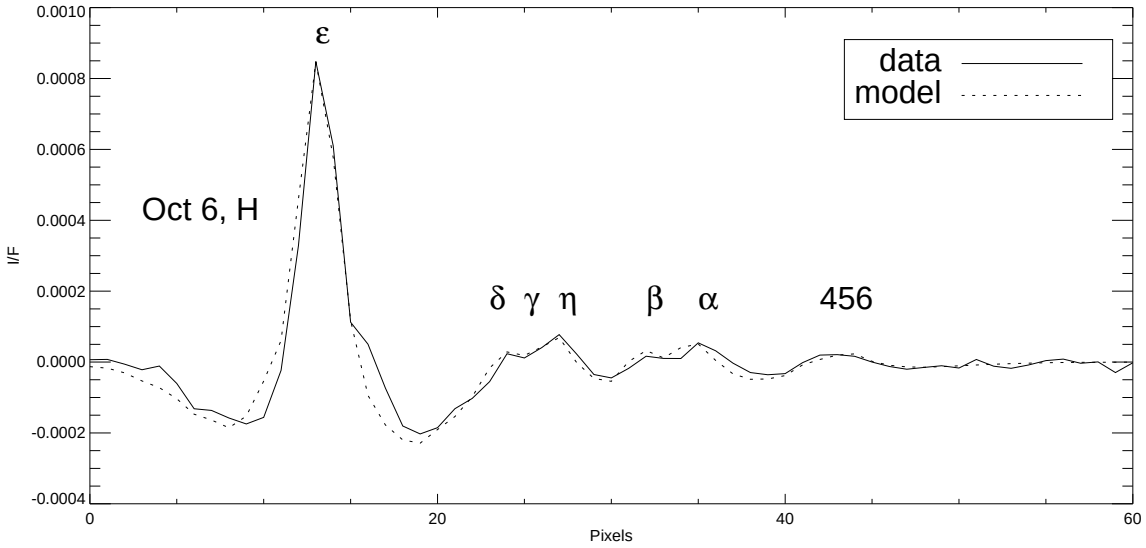
data
model
ε
Oct 6, H
δ γ η β α 456
I/F
Pixels
0.0010
0.0008
0.0006
0.0004
0.0002
0.0000
-0.0002
-0.0004
0
20
40
60

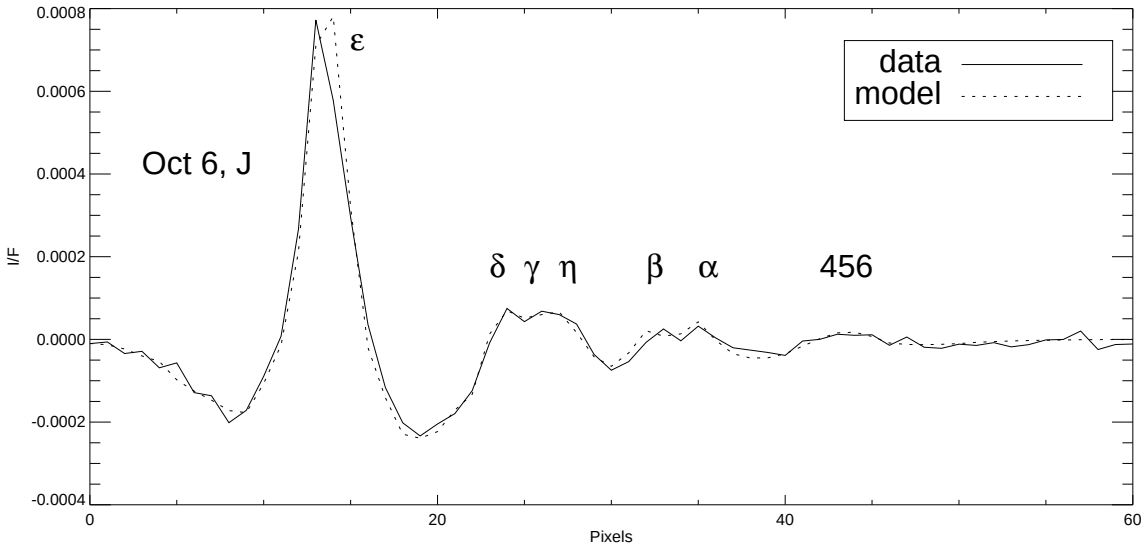
data
model
ε
Oct 6, J
δ γ η β α 456
I/F
Pixels
0.0008
0.0006
0.0004
0.0002
0.0000
-0.0002
-0.0004
0
20
40
60

2003-Oct-5 9:00 UT

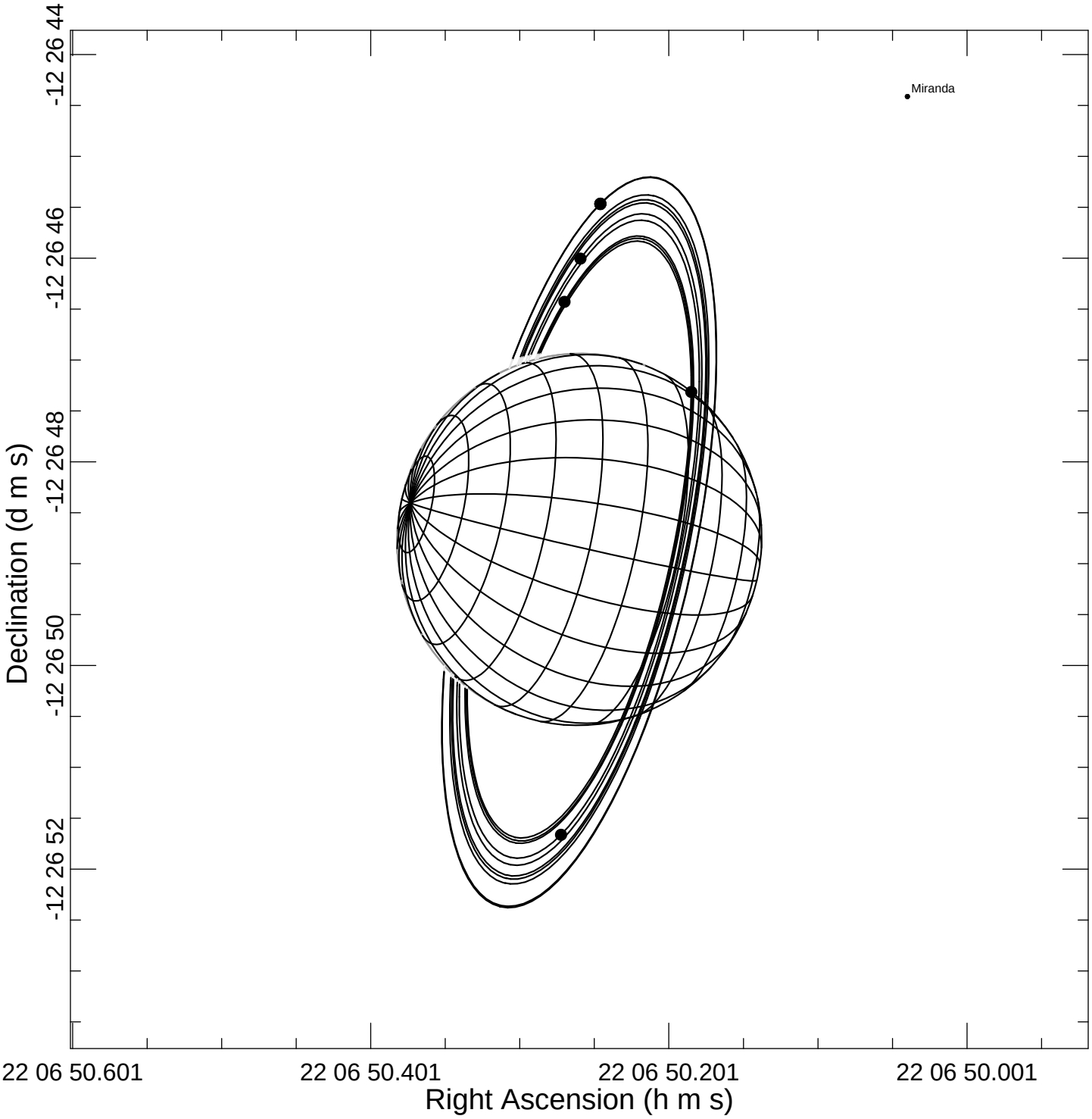

Time (UTC): 2003-OCT-5 09:00
Ephemeris: #4 (URA027 + URA039 + DE405)
Viewpoint: Earth’s center
Moon selection: Miranda-Oberon
Ring selection: 6-Epsilon

Generated by the Uranus Viewer Tool, PDS Rings Node, 08-Jan-04 11:50:10